Journal of Computational and Applied Mathematics 234 (2010) 2287–2296

Contents lists available at ScienceDirect

Journal of Computational and Applied Mathematics

journal homepage: www.elsevier.com/locate/cam

An improved constitutive model for the numerical simulation of semi-solid thixoforming

R. Koeune *, J.-P. Ponthot

Aerospace and Mechanical Engineering Department, University of Liège, Sart-Tilman, 4000 Liège, Belgium

ARTICLE INFO

Article history:
Received 12 September 2008
Received in revised form 20 April 2009

Keywords:
Finite element
Thixoforming
Semi-solid
Constitutive law

ABSTRACT

In order to model thixoforming processes, previous papers presented a thermomechanical one-phase modelling. This first version of the constitutive model revealed several limitations: the model could not degenerate properly to pure solid or liquid behavior nor to free solid suspensions. The aim of this paper was to propose solutions to overcome these limitations.

© 2009 Elsevier B.V. All rights reserved.

1. Introduction

Semi-solid thixoforming is a forming process at temperatures located inside the fusion interval. It relies on a semi-solid microstructure (represented on the micrograph in Fig. 4 and illustrated in Fig. 2) made of globular solid grains more or less connected to each other, thus forming a solid skeleton deforming into a liquid phase. This particular microstructure makes semi-solid materials behave as solids at rest and flow during shearing because the viscosity and the resistance to deformation decrease with shearing, as illustrated in Fig. 1.

In a previous paper [1], we presented a thermomechanical one-phase modelling in order to predict die filling. In this kind of model, the material is regarded as a single continuous phase and the relative displacement between the phases cannot be taken into account. This first version of the constitutive model revealed several limitations: the model could not degenerate properly to pure solid or liquid behavior nor to isolated solid agglomerates. So several enhanced models have been proposed and implemented into the finite element code METAFOR.

2. Description of the proposed models

The basic idea is to extend the Norton–Hoff law to solid hypoelastic formulation, considering the elastic part of the deformation as well as two non-dimensional internal parameters: the **liquid fraction** and the **cohesion degree**.

Nowadays, there is still a dispute over whether thixotropic semi-solid alloys display yield or not. We decided here to use a finite yield stress since a vertical billet does not collapse under its own weight unless the liquid fraction is too high. Furthermore, this choice allows us to predict the residual stresses due to elasticity.

Semi-solid contains both liquid and solid and behaves as a solid or a fluid depending on process conditions. Behavior of liquids and solids under normal pressure are comparable, so we will focus on the deviatoric stresses to look for the main differences between those formalisms.

* Corresponding address: LTAS-non linear mechanics, University of Liege, Chemin des Chevreuils 1, 4000 Liege, Belgium.
E-mail address: r.koeune@ulg.ac.be (R. Koeune).

0377-0427/$ – see front matter © 2009 Elsevier B.V. All rights reserved.
doi:10.1016/j.cam.2009.08.085

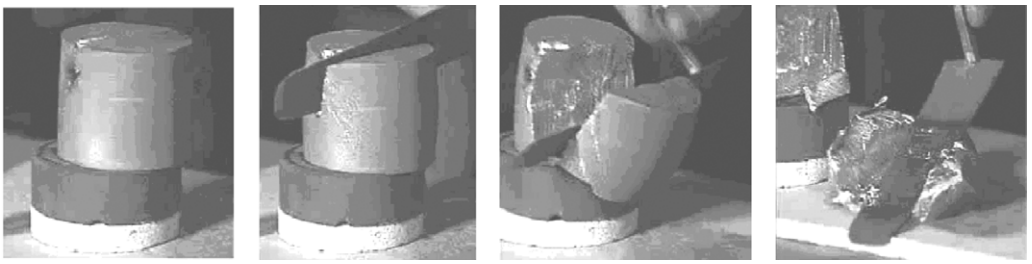

Fig. 1. Photographic sequence illustrating the thixotropic behavior of semi-solid alloy slugs [2].

Liquids resist very weakly to shear and tensile solicitations. Liquids cannot stop themselves shearing because they cannot develop enough restoring force to balance to such a stress (as solids do). That means that any shear stress applied on a liquid leads to steadily increasing strain, thus to a flow. Therefore, it does not make sense to **relate stress** to strain (as it is done for solids), but rather **to strain rate**. In the incompressible linear (Newtonian) case, we have:

$$\text{Liquid approach:}\quad \mathbf{s} = \eta\hat{\mathbf{D}} \tag{1}$$

where $\mathbf{s}$ and $\hat{\mathbf{D}}$ are the deviatoric stresses and strain rate tensor respectively and η is the viscosity.

On the other hand, as a **solid** is deformed beyond a certain level of strain, permanent, non-recoverable or plastic deformation occurs. Thus, the plastic behavior depends on the loading history and is mathematically represented by an **incremental stress–strain relationship**. In the linear (elastic) case, we have:

$$\text{Solid approach:}\quad \overset{\triangledown}{\mathbf{s}} = G\hat{\mathbf{D}} \tag{2}$$

where the operator $\triangledown$ stands for the objective time derivative and G is the shear modulus.

We can see that if the deformation stops ($\hat{\mathbf{D}} \to 0$ which does not mean that there is no strain left), the deviatoric stresses given by the fluid law (Eq. (1)) tends to zero for whatever viscosity. Therefore, the choice of a non-rigid solid formalism is motivated by the fact that such formalism offers the possibility to analyse the residual stresses after unloading and cooling down to room temperature.

Furthermore, if solids are submitted to higher stresses than their plasticity threshold (which decreases if temperature increases), a **plastic flow** is developed and some hardening occurs. At high temperatures both yield strength and strain hardening are really low and the solid material will deform by viscous flow. In this visco-plastic (non-elastic) case, an internal parameter describing the memory of the material is used. It is the equivalent plastic strain $\overline{\epsilon}^{vp}$, defined incrementally by mean of its rate: $\dot{\overline{\epsilon}}^{vp} = \sqrt{2/3\,\mathbf{D}^{vp} : \mathbf{D}^{vp}}$ which is calculated by an extended consistency equation:

$$\overline{\sigma}^{VM} - \sigma_y(\dot{\overline{\epsilon}}^{vp}, \overline{\epsilon}^{vp}) - \eta(\dot{\overline{\epsilon}}^{vp}, \overline{\epsilon}^{vp})\dot{\overline{\epsilon}}^{vp} = 0 \tag{3}$$

where $\overline{\sigma}^{VM} = \sqrt{3/2\,\mathbf{s} : \mathbf{s}}$ is the equivalent von Mises stress, σ_y the yield stress and η is the **apparent viscosity** defined by analogy with liquid formalism. So, the so-called "solid" formalism is not restricted to solid material (at temperature under solidus) and the aim of this work is to develop a constitutive law that is able to describe the thixotropic behavior in the whole range of temperatures occurring during the process. Thus, we are looking for a model that can predict the behavior of a built-up semi-solid material, or of free solid suspensions, or even the elastic behavior (to describe the cooling down to room temperature and thus the residual stresses).

The internal parameters of liquid fraction f_l and cohesion degree λ have been introduced to simulate the complex rheology of semi-solid materials, under both steady-state and transient conditions. For example, the peak of viscosity at start of a fast loading should be appropriately reproduced.

Thus, the new extended consistency equation is written as

$$\overline{\sigma}^{VM} - \sigma_y(f_l, \lambda, \dot{\overline{\epsilon}}^{vp}, \overline{\epsilon}^{vp}) - \eta(f_l, \lambda, \dot{\overline{\epsilon}}^{vp}, \overline{\epsilon}^{vp})\dot{\overline{\epsilon}}^{vp} = 0. \tag{4}$$

Different models based on this formulation have been proposed. Both internal parameters introduced in the initial work have been enhanced and the evolution of the yield stress and the apparent viscosity with the internal parameters have been described by several hardening and viscosity laws.

2.1. Initial model [1]

2.1.1. Cohesion degree

The first internal parameter is the **cohesion degree** λ and is illustrated in Fig. 2. During the process, the material structure changes with the strain history due to the agglomeration of the particles and the breaking of the grain bonds. So, λ is a

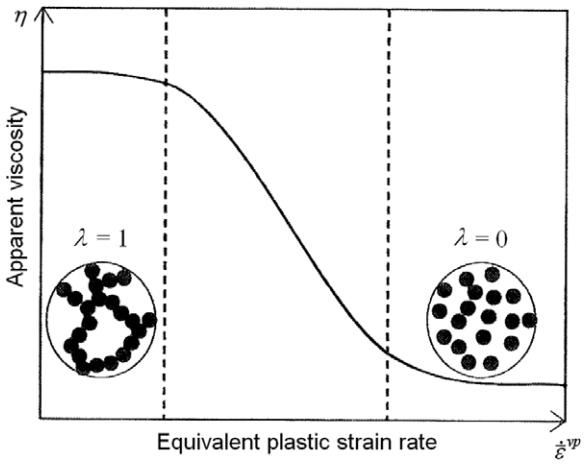

Fig. 2. Illustration of the cohesion degree.

structural parameter that characterizes the degree of build-up in the microstructure and can take values between 0 and 1: $\lambda = 1$ if the structure is fully built-up and $\lambda = 0$ if the structure is fully broken.

Then, the evolution of the structural parameter λ is described by a differential equation that describes the kinetics between the agglomeration of the solid grains and the destruction of the solid bonds due to shearing (generalized expression of common equations published in [2] and [3]):

$$\dot{\lambda} = \underbrace{a(1-\lambda)}_{build-up} - \underbrace{b\lambda(\dot{\bar{\epsilon}}^{vp})^c e^{d\dot{\bar{\epsilon}}^{vp}}}_{breakdown} \tag{5}$$

where a, b, c and d are material parameters.

We can define the steady-state (or equilibrium) cohesion degree λ_e, at which:

$$\dot{\lambda}(\lambda_e) \to 0 \Leftrightarrow \lambda_e = \frac{a}{a + b(\dot{\bar{\epsilon}}^{vp})^c e^{d\dot{\bar{\epsilon}}^{vp}}}. \tag{6}$$

2.1.2. Liquid fraction

The second internal parameter is the liquid fraction f_l. It depends only on the temperature by the steady-state Scheil [4] equation:

$$f_l = \left(\frac{T - T_s}{T_l - T_s}\right)^{\frac{1}{r-1}} \tag{7}$$

where r is the equilibrium partition ratio, T_s and T_l are the solidus and liquidus temperatures respectively.

2.1.3. Viscosity law

The basic Norton–Hoff law reads

$$\eta = k(\dot{\bar{\epsilon}}^{vp})^{m-1}. \tag{8}$$

This law has been adapted to thixotropic behavior by introducing both internal parameters via the viscosity parameters k and m. The viscosity increases with the cohesion degree by an empirical law established in [3], and increases exponentially with the solid fraction [5]. Thus, we have

$$\begin{cases} k = k_1 e^{k_2(1-f_l)}\, e^{k_3\lambda} \\ m = (m_1 + m_3\lambda^2 + m_4\lambda)\, e^{m_2(1-f_l)} \end{cases} \tag{9}$$

where k_1, k_2, k_3, m_1, m_2, m_3 and m_4 are material parameters.

2.1.4. Yield and isotropic hardening law

An extended Shima and Oyane [6] isotropic hardening law has been used. As a liquid does not display yield, this law takes into account a decrease of the yield stress with liquid fraction elevation. A term of linear hardening (which remains small at

high temperatures) has been added to initial Shima and Oyane law in order to meet a classical linear hardening law at solid state ($f_l = 0$). It is expressed by

$$\sigma_y = (1 - f_l)^{h_2} \ (\sigma_y^0 + h_1 \, \overline{\epsilon}^{vp}) \tag{10}$$

where σ_y^0 is the initial yield stress, h_1 and h_2 are material parameters.

2.2. Enhanced proposed model

The initially presented model suffers a few drawbacks that we will try to make up.

2.2.1. Cohesion degree

In the previous model, the liquid fraction and the cohesion degree are defined independently, which is not physically based. Actually, the cohesion degree depends on the liquid fraction since it should be zero at liquid state, and unity at solid state. There can be no solid bonds at a fully liquid state and a solid structure must be fully built-up. So, this model is not extensible to pure solid or liquid behavior.

To overcome this limitation, we can use a cohesion degree that depends on the liquid fraction. By solving the differential equation (5), we can adapt it and introduce the liquid fraction in order to degenerate properly to a pure solid or liquid state behavior. We get

$$\dot{\lambda} = a(1 - f_l)(1 - \lambda) - b f_l \lambda (\dot{\overline{\epsilon}}^{vp})^c \, e^{d\dot{\overline{\epsilon}}^{vp}} \quad \text{with } \lambda_{init} = 1. \tag{11}$$

Thus, we have $\lambda_e = \frac{a(1-f_l)}{a(1-f_l) + b f_l \lambda (\dot{\overline{\epsilon}}^{vp})^c \, e^{d\dot{\overline{\epsilon}}^{vp}}} \ \rightarrow \ 1 - f_l$ if $f_l \ \rightarrow \ 0$ or 1.

2.2.2. Liquid fraction

We propose to use a new internal parameter: the **effective liquid fraction** f_l^{eff} which excludes the liquid that is entrapped inside the solid grains (see micrograph in Fig. 4) and that does not contribute to the flow. With the breaking of the solid bonds some of this entrapped liquid is released, so f_l^{eff} is expressed in terms of the cohesion degree as $f_l^{eff} = f_l(1 - \lambda)$. The liquid fraction can be replaced by the effective one in any viscosity and hardening law, according to the user choice.

Thereby, the two internal parameters of liquid fraction and cohesion degree are no longer independent to each other.

2.2.3. Viscosity law

The previous viscosity law is not extensible to a fully broken structure. In this case, $\lambda = 0$ and cannot act on the apparent viscosity anymore, this last one keeps increasing with the strain rate (see [1]). So, we propose a combination between the behavior of a built-up structure described by (8) and (9) and the low viscosity of free solid suspensions (whose behavior is considered as Newtonian so far). This leads to a smooth cubic interpolation between both behaviors, illustrated in Fig. 3:

$$\eta = \eta_{\text{susp}} + \lambda^2(3 - 2\lambda)(\eta_{\text{skel}} - \eta_{\text{susp}}) \tag{12}$$

where $\eta_{\text{susp}} = k_1$ and $\eta_{\text{skel}} = k(\dot{\overline{\epsilon}}^{vp})^{m-1}$ are the viscosity of the free solid suspensions and the solid skeleton respectively, with k and m described by equation (9).

2.2.4. Yield and isotropic hardening law

In the previous work, several trials of introducing the cohesion degree into the extended Shima and Oyane isotropic hardening law (10) had been made but were not efficient in term of computation time [1]. Here, we propose to use the new internal parameter f_l^{eff} instead of the liquid fraction in the hardening law, this introduces the cohesion degree.

$$\sigma_y = (1 - f_l^{eff})^{h_2} \ (\sigma_y^0 + h_1 \, \overline{\epsilon}^{vp}) = (1 - f_l(1 - \lambda))^{h_2} \ (\sigma_y^0 + h_1 \, \overline{\epsilon}^{vp}). \tag{13}$$

2.3. Micro–macro model

This model proposed in [7] has been implemented in METAFOR. It individualizes the mechanical role of the non-entrapped and entrapped liquid and of the solid bonds and the solid grains in the deformation mechanisms. The microstructure is represented by "**coated inclusions**" (Fig. 4), the inclusion is composed of the solid grains and the entrapped liquid whereas the coating, called the "**active zone**" is composed of the solid bonds and the non-entrapped liquid. In this case, we neglect the hardening. Also, the use of the effective liquid fraction does not make sense and the liquid fraction is calculated by the Scheil equation (7).

2.3.1. Cohesion degree

The cohesion degree can also be regarded as the solid fraction of the active zone. Here, we assume that the structure has enough time to reach an equilibrium and the cohesion degree is a steady-state explicit function of the strain rate. This

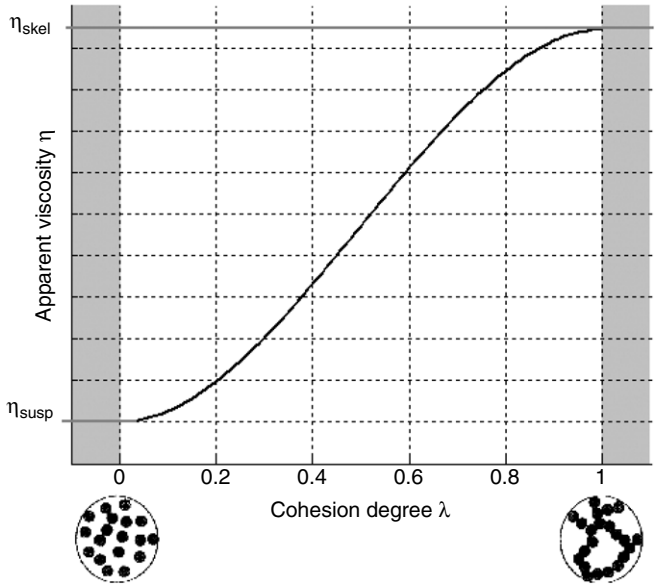

Fig. 3. Illustration of the enhanced viscosity law.

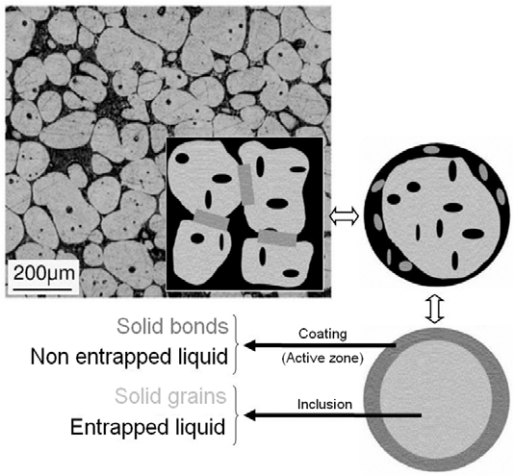

Fig. 4. Microstructure of semi-solid alloy and schematic representation in the micro–macro model [7].

function is obtained by solving Eq. (11) and neglecting the time dependent term. Also, it is assumed that above a critical liquid fraction f_c the solid phase appears as isolated agglomerates so that λ is zero. Overall, the cohesion degree is written as

$$\lambda = \begin{cases} \dfrac{1-f_l}{1-f_l\left(1-\frac{b}{a}(\dot{\bar{\epsilon}}^{vp})^c e^{d\dot{\bar{\epsilon}}^{vp}}\right)} & \text{if } f_l < f_c \\ 0 & \text{otherwise.} \end{cases} \tag{14}$$

2.3.2. Viscosity law

To determine the viscosity, a self-consistent approximation is used at two scales. The apparent viscosity is deduced from the apparent viscosities η_A and η_I of the active zone and of the inclusion respectively that are both calculated from the liquid and solid behavior, according to equation (15) to (17):

$$\eta = \eta_A + (1-f_A)(\eta_I - \eta_A)A_I \tag{15}$$

$$\eta_A = k_l + \lambda\left(k_s(\dot{\bar{\epsilon}}^s_A)^{m-1} - k_l\right)A^s_A \quad \text{where } \dot{\bar{\epsilon}}^s_A = A^s_A\frac{1-A_I(1-f_A)}{f_A}\dot{\bar{\epsilon}}^{vp} \tag{16}$$

Table 1
Material parameters for Sn-15%wt Pb alloy.

Young modulus: $E = 38 - 0.1T$ (GPa) Thermal expansion coefficient: $23.5E^{-6}$ (1/K)	Shear modulus: $G = \frac{E}{2.8}$ Conductivity: 60 (W/m °C)	Density: $7.7E^3$ (kg/m^3) Heat Capacity: 220 (J/kg °C)
Equilibrium partition ratio: $r = 1.5$	Solidus: $T_s = 183$ (°C)	Liquidus: $T_l = 210$ (°C)
Cohesion degree: $a = 0.035$ (1/s); $b = 0.15$; $c = 1.5$ (s); $d = 0.001$; $\lambda_{initial} = 1$; $f_c = 0.6$		
Viscosity : $k_1 = 0.45$ (Pa); $k_2 = 0.1$; $k_3 = 12.173$; - *Initial model*: $m_1 = 3.95$; $m_2 = 0.1$; $m_3 = 1.86$; $m_4 = -3.77$ - *Enhanced model*: $m_1 = 1$; $m_2 = 0.1$; $m_3 = m_4 = 0$ - *Micro-macro model*: $k_s = 1$(MPa); $k_l = 1.81E - 3$(Pa); $m = 0.43$; $f_A = 0.007$		
Hardening:$h_1 = 11.43$(MPa);$h_2 = 2.5$;$\sigma_y^0 = 6.86$(MPa)		

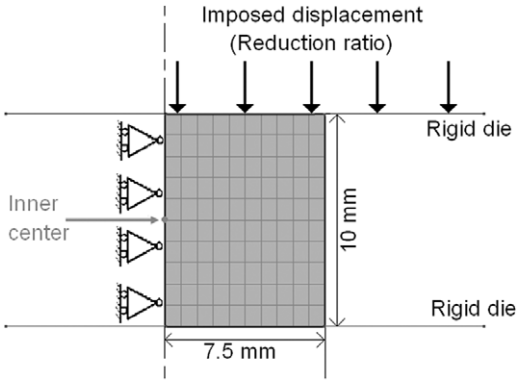

Fig. 5. Description of the compression test.

$$\eta_I = k_l + \frac{1 - f_l - f_A\lambda}{1 - f_A}\left(k_s(\dot{\bar{\epsilon}}_I^s)^{m-1} - k_l\right)A_I^s \quad \text{where } \dot{\bar{\epsilon}}_I^s = A_I^s A_I \dot{\bar{\epsilon}}^{vp} \tag{17}$$

where A_l^s, and A_A^s are the localisation variables of the solid phase in the inclusions and in the active zone respectively and A_I is the localisation variable of the inclusions in the global semi-solid material. These variables depend on the three viscosities η_A, η_I and η, which gives a system of 3 equations for 3 unknowns that is solved numerically by Newton–Raphson iterations.

3. Numerical simulations

In all simulations, the material under study is a Sn-15%wt Pb alloy. The material parameters for Sn-15%wt Pb have been found in the literature [3,7,8] and are detailed in Table 1.

3.1. Compression test

As a first validation of the proposed material models, a simple 2D axisymmetric test, that consists in the compression of a cylinder (described in Fig. 5), has been simulated and compared to available results on compression load (Kang [8]). The cylinder is 10 mm high and has a radius of 7.5 mm. One section is discretized using a 10 by 10 mesh. The die velocity and temperature are 38 mm/s and 150 °C respectively. The friction coefficient is 0.3 and the initial temperature is such as the initial liquid fraction will be 37%.

3.1.1. Isothermal analysis

In a first step, isothermal simulations have been conducted. In Fig. 6, the loading pressure predicted by the enhanced model shows good agreement with the reference [8], while the lack of hardening in the micro–macro model causes an underestimation of the load. Since it does not consider the entrapped liquid, the initial model underestimates the solid fraction and thus the initial yield stress and loading pressure.

3.1.2. Thermomechanical analysis

Then, thermomechanical simulations have been carried out. In this case, the loading pressure is a bit higher than under isothermal conditions due to the contact with the colder die.

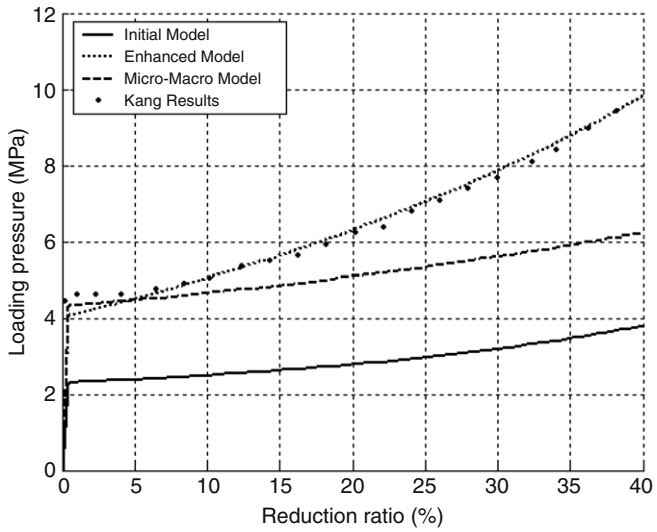

Fig. 6. Loading pressure (isothermal models).

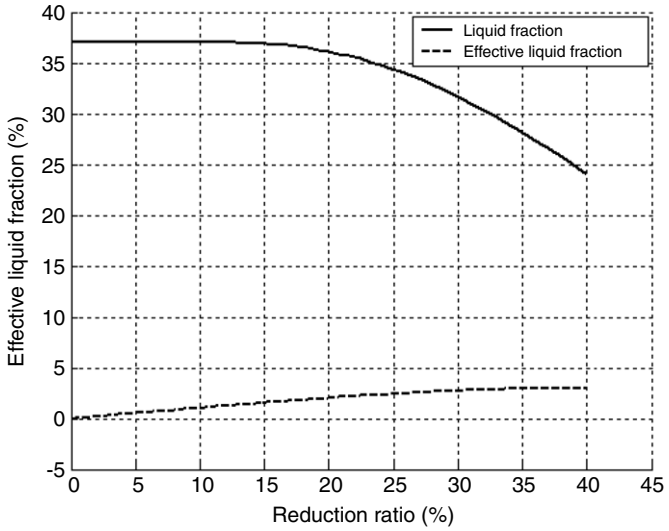

Fig. 7. (Effective) Liquid fraction evolutions.

In Fig. 7, we can see the evolution of the liquid fraction compared to the new internal parameter of effective liquid fraction at the inner center of the cylinder (see Fig. 5). Before loading, the initial liquid fraction and cohesion degree are set to 37 % and 1 respectively. Thus, the effective liquid fraction starts at a value of 0. During the forming process, some solidification occurs ($f_l \downarrow$) due to the thermomechanical contact with the cold die. At the same time, the structure is broken down by shearing, and the cohesion degree decreases. Overall, the effective liquid fraction increases due to the release of some entrapped liquid.

3.1.3. Residual stresses

During a third step, the residual stresses have been computed using a mechanical analysis with imposed temperature evolution. The calculation is then made in two successive steps. The forming stage with a uniform drop of 5 °C representing the die contact is followed by the unloading and the cooling down to room temperature.

In Fig. 8, the cohesion degree at the inner center of the cylinder is compared for all proposed formulations. During the forming process, the drop of temperature causes a decrease of the liquid fraction. Thus, the enhanced formulation of Eq. (11), which takes the liquid fraction into account, predicts a higher cohesion degree than Eq. (5). In the case of the steady-state formulation of Eq. (14), λ drops as soon as the deformation starts because the model assumes that the structure has enough time to adapt to the new strain rate state, and then it goes back to 1 as soon as the die is removed. During the cooling down stage, the formulation of Eq. (5), which does not depend on the temperature, predicts a slow recovery of the semi-

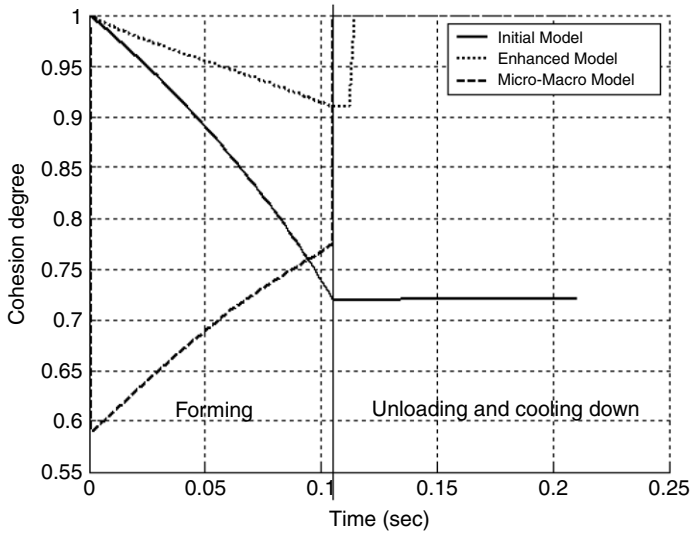

Fig. 8. Cohesion degree for different models with unloading and cooling down.

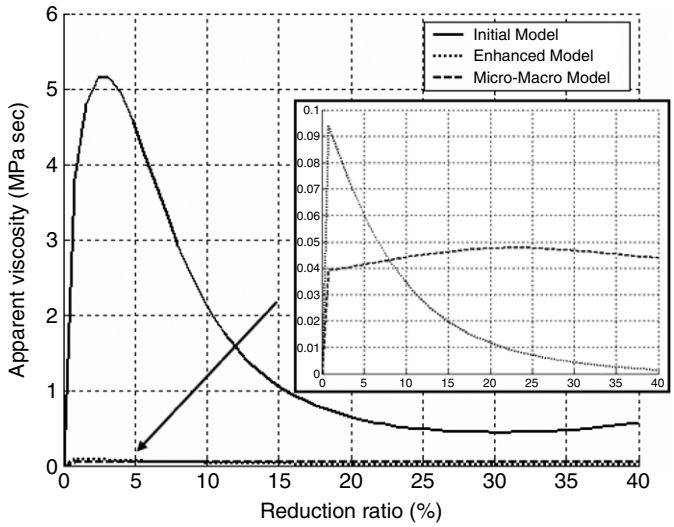

Fig. 9. Apparent viscosity for different models at high compression rate ($V_{die} = 500$ mm/sec).

solid material, while Eqs. (11) and (14) predict a fully built-up structure ($\lambda = 1$) when the solidus is reached, which makes physical sense.

The distribution of residual stresses is not represented here, but we can say that both initial and enhanced calculations predicted quiet uniform distribution of von Mises stresses of 1.75 MPa in the heart of the billet, but a high stresses gradient on the edge (maximum of 20 MPa). The micro–macro model predicts residual stresses that does not exceed 5.2 MPa.

3.1.4. Dynamic analysis

Finally, the influence of die velocity has been studied using a mechanical analysis with a uniform imposed drop of temperature of 5 °C. Fig. 9 represents the evolution of the apparent viscosity at the center of the billet.

At the start of the loading, we can observe a peak of viscosity for the first two proposed models. This peak is much lower in the case of the enhanced law because of the lower strain rate sensitivity m. Then, a drop of viscosity occurs with loading. In the case of the micro–macro law, this drop of viscosity does not happen. In fact, in the present case, the strain rate is too low to reach the threshold that is discussed in [7].

For higher die velocities, we can also see that, beyond a certain level of deformation, the viscosity starts to increase in the case of the initial model while it tends to zero in the enhanced model and it starts to reduce in the micro–macro law. If the solid network keeps breaking down, the initial viscosity law will raise tremendously while the enhanced one will tend to zero and the micro–macro viscosity would drop drastically as observed in [7].

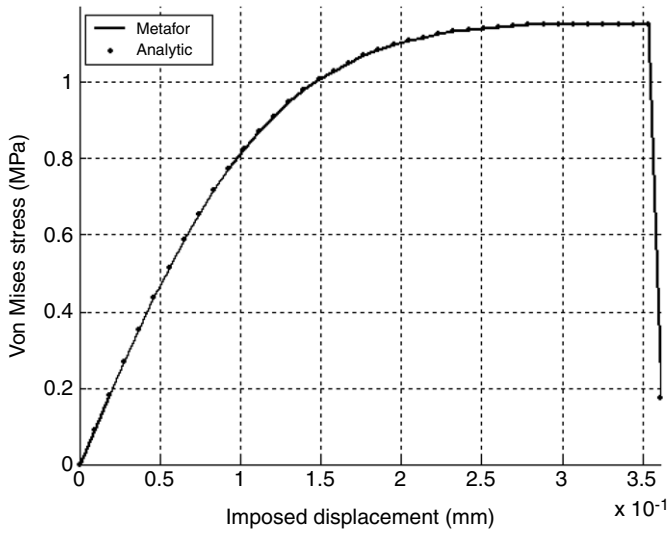

Fig. 10. von Mises stress (micro–macro model).

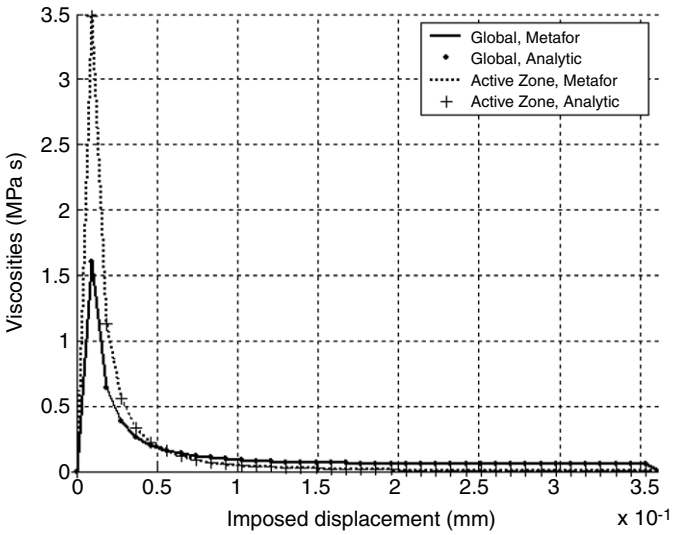

Fig. 11. Viscosities (micro–macro model).

3.2. Simple shear test

We also used the simple 2D plane strain isothermal shear test of a mono-element (1 by 1 mm), for which we know the analytic solution[1], to validate the micro–macro model. In this theoretical case, we assume there is no yield stress. The liquid fraction is 50%.

As we look at the results in terms of the evolution of the equivalent stress in Fig. 10, the global viscosity and the viscosity in the active zone (all uniform on the piece) in Fig. 11, we can see that the computed results are in agreement with the "pseudo-analytical" solution.

Beyond a critical deformation, the consistency of the solid skeleton gets too low to hold the deformation, a more dispersed suspensions having a fluid-like behavior is thus obtained, and, in the calculation, a strong decrease of viscosity is observed. The transition between "solid" and "liquid" regime predicted by the model is too drastic (as we can see the stresses and the viscosities dropping down extremely fast). This effect is only due to the formulation of the self-consistent model and it does not describe correctly the real behavior. Indeed, the real mechanisms of the percolation effect are more complex and softer.

[1] Note that the resolution of the system of equations of the micro–macro model cannot be solve analytically, so the so-called "analytic" solution should be more appropriately called "pseudo-analytic".

4. Conclusion

In summary, this paper concerns the development of improved constitutive models for semi-solid thixoforming. The new models are described and tested with academic examples. The initial law limits have been overcome by the new proposed model without adding any new material parameter. Now the model can degenerate properly to pure solid or liquid as well as free solid suspensions behavior. Residual stresses, but also thermomechanical and transient behavior occurring in a thixoforming process have been modelled. The micro–macro model gives also good results. The next steps of the research are the accurate validation of the model by comparison of more sophisticated simulations to experimental data and particularly the identification of the material parameters.

References

[1] R. Koeune, J.P. Ponthot, Thermomechanical one-phase modeling of semi-solid thixoforming, in: E. Oate M. Papadrakakis B. Schrefler (Eds.), Proc. of the Int. Conf. on Computational Methods for Coupled Problems in Science and Engineering, Ibiza, 2007, pp. 166–169.
[2] H.V. Atkinson, Modelling the semisolid processing of metallic alloys, Prog. Mater. Sci. 50 (2005) 341–412.
[3] G.R. Burgos, A.N. Alexandrou, V.M. Entov, Thixotropic rheology of semisolid metal suspensions, J. Mater. Process. Technol. 110 (2001) 164–176.
[4] O. Lashkari, R. Ghomashchi, The implication of rheology in semi-solid metal processes: An overview, J. Mater. Process. Technol. 182 (2007) 229–240.
[5] M. Modigell, J. Koke, Rheological modelling on semi-solid metal alloys and simulation of thixocasting processes, J. Mater. Process. Technol. 111 (2001) 53–58.
[6] S. Shima, M. Oyane, Plasticity theory for porous metals, Int. J. Mech. Sci. 18 (1976) 285–291.
[7] V. Favier, C. Rouff, R. Bigot, M. Berveiller, M. Robelet, Micro-macro modeling of the isothermal steady-state behaviour of semi-solids, Int. J. Forming Process. 7 (2004) 177–194.
[8] C.G. Kang, J.H. Yoon, A finite-element analysis on the upsetting process of semi-solid aluminum material, J. Mater. Process. Technol. 66 (1997) 76–84.